This paper was resubmitted to Journal Geophysical Research because the referee has suggested to change the title.

Electrostatic Wave Generation and Transverse Ion Acceleration by Alfvénic Wave Components of BBELF Turbulence

Nagendra Singh[1], George Khazanov[2], Ali Mukhter[1]

1. Department of Electrical and Computer Engineering, University of Alabama, Huntsville, Alabama, 35899, USA.

2. NSSTC, Marshal Space Flight Center, Huntsville, AL, 35812

Abstract

We present results here from 2.5-D particle-in-cell simulations showing that the electrostatic (ES) components of broadband extremely low frequency (BBELF) waves could possibly be generated by cross-field plasma instabilities driven by the relative drifts between the heavy and light ion species in the electromagnetic (EM) Alfvénic component of the BBELF waves in a multi-ion plasma. The ES components consist of ion cyclotron as well as lower hybrid modes. We also demonstrate that the ES wave generation is directly involved in the transverse acceleration of ions (TAI) as commonly measured with the BBELF wave events. The heating is affected by ion cyclotron resonance in the cyclotron modes and Landau resonance in the lower hybrid waves. In the simulation we drive the plasma by the transverse electric field, E_y, of the EM waves; the frequency of E_y, ω_d, is varied from a frequency below the heavy ion cyclotron frequency, ω_h, to below the light ion cyclotron frequency, ω_i. We have also performed simulations for E_y having a continuous spectrum given by a power law, namely, $|E_y| \sim \omega_d^{-\alpha}$, where

the exponent = _, 1, and 2 in three different simulations. The driving electric field generates polarization and E B drifts of the ions and electrons. When the interspecies relative drifts are sufficiently large, they drive electrostatic waves, which cause perpendicular heating of both light and heavy ions. The transverse ion heating found here is discussed in relation to observations from Cluster, FAST and Freja.

1. Introduction

In recent years, two quite different low-frequency (LF) wave phenomena have been identified in the auroral plasma and they are the electromagnetic ion cyclotron (EMIC) waves and the broadband ELF (BBELF) waves [Boehm et al., 1990; Bonnell et al., 1996; Kintner et al, 1996; Wahlund et al., 1998; 2003; Klatt et al., 2005]. The EMIC waves occur in certain frequency bands in a multi-ion plasma [e.g. see Erlandson et al., 1994]. On the other hand, BBELF waves appear without any distinctly identifiable features in the frequency spectrum extending from the lowest frequency Alfvénic waves to proton plasma and/or lower hybrid (LH) frequency. The low-frequency components in the BBELF waves are electromagnetic, especially below the heavy ion cyclotron frequency in a multi-ion plasma, and they become increasingly electrostatic with increasing frequency. For the purpose of easy reference, we call the EM and ES components of the BBELF waves EMELF and ESELF waves. For our purposes in this paper the EMELF waves include EMIC waves as well.

The data from the Freja satellite clearly demonstrated that when EMELF waves dissipate at altitudes near h~ 1700 km, some of the wave energy goes in transverse heating of ions [Louarn et al., 1994; Wahlund et al., 1994; Erlandson et al., 1994]. Erlandson et al. [1994] reported interesting examples of EMIC waves in two bands, one below the O^+ cyclotron frequency and

the other between He^+ and H^+ cyclotron frequencies, the latter correlating with preferential heating of O^+ ions. Results from FAST also show strong connection between EMELF waves and ion heating [e g., see Chaston et al., 2004]; the ions' pitch angles measured from FAST at altitudes near h~3500 km indicate local transverse heating and most energetic ions are the heavy O^+ ions.

In a series of recent satellite observations from the Polar satellite, it is demonstrated that plasma electrodynamics along the field lines threading through the pole-ward boundary of the auroral oval and the plasma sheet boundary layer is dominated by Alfvén waves [Wygant et al., 2000, 2002; Keiling et al., 2005; Angelopoulos et al., 2002]. Specifically Wygant et al. [2002] show that narrow-structured Alfvén waves, believed to be the kinetic Alfvén Waves (KAWs) are embedded in much wider Alfvén wave structures, which have long wavelengths across the ambient magnetic field. It is reported that such waves accelerate electrons parallel to the ambient magnetic field and ions perpendicular to it.

Wahlund et al. [2003] have reported observation BBELF waves from Cluster at a high geocentric altitude of ~ 4-5 R_e showing that features of the wave are similar to those seen from rocket and low-altitude satellites [Boehm et al., 1990; Wahlund et al., 1994; 1998; Stasiewicz et al. 2000]. Figure 1a shows the frequency spectrum of the fluctuations in the perpendicular electric field of the ELF waves. The two curves in the figure, one with lower power level in a quiet region and the other curve in an immediately following active region with intense waves during the course of traversal of Cluster show the increase in the electric field wave power by one to three orders of magnitude in the active region over the entire band of frequency shown.

Wahlund et al. [2003] point out that for the spatial scales of the waves, the Doppler shift due to satellite velocity is not significant, unlike in the case of Freja [Stasiewicz et al., 2000] and FAST [Chaston et al., 2004] observations. So the frequencies shown are in the rest frame of the plasma. The power in the magnetic component during the intense wave period increases below 2 Hz, and only below 0.4 Hz as much as the electric power (Figure 1b). Although the spectrum in Fig. 2a is only up to 10 Hz, Wahlund et al. [2003] point out that the enhancement extends up to the low-frequency cut-off of the auroral hiss emissions observed near 300-400 Hz. Furthermore, they found that $\delta E/\delta B$ steadily increases above 0.4 Hz, and below this frequency it is close to $9\cdot10^6$-$3\cdot10^7$ m/s, the range of the Alfvén velocity during the observation time. It is worth mentioning that O^+ cyclotron frequency is 0.46 Hz and for H^+ it is ~ 7.5 Hz. Thus, the low-frequency components below ~0.4 Hz are Alfvénic waves while at higher frequencies the waves become increasingly electrostatic. Klatt et al. [2005] recently reported observations of ELF waves, showing a direct relation between the Alfvénic waves and electrostatic noise; the latter coincides with the peak in the transverse electric and magnetic fields of the former. Since the peak of the magnetic field perturbations coincides with the maximum gradient in the current density associated with the DAWS, Klatt et al. [2005] have suggested that the noise, which extends both below and above the lower hybrid frequency, might be generated by current- advective shear-driven CASDI instability (CASDI) [Seyler and Xu, 2003]. Even the Observation from Freja shows a direct connection between EMELF waves and high frequency electrostatic waves [Wahlund et al., 1994; Erlandson et al., 1994]. Wahlund et al. [1998] suggested that as the EMELF waves propagate down, they emit the electrostatic waves. They also suggested that the electrostatic waves could be ion-acoustic waves.

Khazanov et al. [1997a,b] have theoretically demonstrated that the Alfvén wave-driven drifts of electrons and ions in a multi-ion plasma could generate high-frequency electrostatic waves even when electron and ion temperatures do not satisfy the condition for the existence of ion-acoustic waves, namely, $T_e>3T_i$. The high-frequency mode generated by this process is lower hybrid waves, which heats ions transversely and electrons parallel to the ambient magnetic field. Singh and Khazanov [2004] showed by means of 2.5-D PIC simulations, that Alfvén wave-driven drifts could generate broadband electrostatic turbulence covering range of frequency from the ion cyclotron harmonics to the LH frequency depending on the relative densities of heavy and light ions. For low densities of the heavy ions, the electrostatic turbulence develops a distinct peak near the LH frequency. As the heavy ion density increases, the peak broadens covering the ion cyclotron harmonics.

The purpose of this paper is to extend the work of Khazanov et al. [1997a,b] and Singh and Khazanov [2004] by considering a range of frequencies of the EMELF waves driving the plasma. First we consider monochromatic coherent waves, whose frequencies vary from below the heavy ion cyclotron frequency Ω_h to below the light ion cyclotron frequency Ω_i in different simulations. In view of the broad broadband EMELF waves seen in satellite observations [Erlandson et al., 1994; Wahlund et al., 2003], we also consider driving fields having a power law spectrum. In the latter case we find that the impulsive nature of the driving electric field in the time-domain, generates large amplitude electrostatic waves causing a large transverse ion heating.

2. Method of Simulation

We use a standard 2.5-D particle-in-cell code [Birdsall and Langdon, 1985], which we have described in previous studies [Singh and Leung, 1999, Singh, 2000]. Specifically we simulate 2-dimensional plasma of dimension L_xxL_y in the x-y plane. The ambient magnetic field B_o has only the z- component in all the simulations reported here. In a set of three simulations from R-1 to R-3, plasma is driven by a monochromatic sinusoidal electric field given by

$$\mathbf{E_y} = \mathbf{a_y}\ F_a(t)\, E_o \sin(\omega_d t), \qquad F_a(t) = \mathrm{erfc}(t/\tau_s)\ , \tag{1}$$

in which the driving wave frequency ω_d is varied from run to run (R1-R3) ranging from below the heavy-ion cyclotron frequency ω_h to just below the light-ion cyclotron frequency ω_i. The plasma has a heavy ion species along with the light ions; the relative density of the heavy ions is 10%. The driving field amplitude E_o is mentioned while discussing the simulation runs. $F_a(t)$ is an adiabatic start function which allows $E_y(t)$ to grow slowly over a time period τ_s to reach the steady state amplitude E_o. τ_s is several times the driving wave period of the heavy ions. If τ_s is not sufficiently long or when $F_a(t)=1$, the response of the ions contain spurious oscillations. In order to economize computing time, we have used ion masses which are not real; we have used $M_i/m=400$, where M_i is the light ion mass and m is electron mass. For the heavy ion mass, we used $M_h/M_i=4$. In the other set of three simulations (R4-R6) the monochromatic driving electric field is replaced by a broadband spectrum covering the frequency range from below ω_h to ω_i. The features of the power-law frequency spectra in these simulations are discussed later. The size of the simulation box is $L_x \times L_y = 256 \times 256\, \lambda_d^2$. We employed 25 electron–ion pairs per cell with cell size λ_dxλ_d, and $\omega_e/\omega_{pe}=1$, where λ_d is the Debye length, and ω_e and ω_{pe} are the electron

cyclotron and plasma frequencies, respectively. We used a time step $\Delta t=2\pi/32$. In the PIC code and our following discussions we use normalized quantities as follows: distances are normalized in the units of λ_d, velocity in units of electron thermal velocity a_{eo}, time in units of the inverse of electron plasma frequency ω_{peo}, electric potential in units of $\phi_n=T_o/e$, and electric field in units of En = _n|_d, where $\lambda_d=a_e/\omega_{pe}$, and $a_{eo}=(T_o/m)^{1/2}$. Ion thermal velocities are likewise defined by $a_{\_o}=(T_\_/M_\_)^{1/2}$, where _ denotes the ion species. T_o is the initial plasma temperature, and it is the same for the electrons as well as the light and heavy ions.

3. Numerical Results

First we present results from simulations, in which the driving EMELF waves are monochromatic. Since the EMELF components of EMIC and BBELF waves overlap in frequency spectrum, such simulations could be relevant to TAI by both EMIC as well as BBELF waves. The monochromatic simulations are followed by discussion of results from simulations driven by broadband EMELF waves. We not only discuss here TAI, but also the generation of ES waves, which are an integral part of the events of EMIC waves and of course BBELF waves observed from satellites.

3.1 Monochromatic Driving Wave

The results from run R-1 are physically analogous to previously reported simulations [Singh and Khazanov, 2004], except that heavy ion mass is $M_h=4M_i$, in contrast to $M_h=9M_i$ in the previous

study. In R-1 we have wave frequency $\omega = 0.75\Omega_h = 0.1875\Omega_i$. Figure 2a shows the temporal evolution of the wave amplitude as seen in the electrostatic potential ϕ (t) at the mid point ($L_x/2$, $L_y/2$) of the simulation region. The unit of ϕ is T_e/e and the time on the horizontal axis is labeled in units of light ion cyclotron period τ_{ci}. The evolution of perpendicular temperature of the heavy ions, $T_{\perp h}$, and of the light ions, $T_{\perp i}$, as well as of the parallel temperatures of the ions and electrons are plotted in Figure 2b. Since the ambient magnetic field is purely perpendicular to the plane of the simulation, as expected the parallel temperatures remain constant at the normalized value of unity. As the driving field $E_y(t)$ grows in the simulation according to the scheme of adiabatic start (see eq. (1)), the amplitude of noise in the electrostatic potential grows. This growth is caused by the *instabilities* generated by the relative drifts between light and heavy ions in the driving field E_y. As an example, the evolution of the E×B drift, V_{xh}, and the polarization drift, V_{yh}, of the heavy ions are plotted in Figure 2c. When $E_y(t)$ reaches its steady oscillation as $E_o\sin(\omega t)$, the waveforms of the drift velocities match the theoretical drifts given by

$$V_{xs}=[1/(1-\omega^2/\Omega_s^2)]\,(E_o/B_o)\sin(\omega t), \qquad (2)$$

$$V_{ys}=[(\omega/\Omega_s)/(1-\omega^2/\Omega_s^2)]\,((E_o/B_o)\cos(\omega t), \qquad (3)$$

where the subscript ‘s’ stands for the ion species with s=h(i) for heavy (light) ions. In the steady state, the amplitudes of V_{xh} and V_{yh} are $0.57a_{eo}$ and $0.42\ a_{eo}$, respectively, and they match well with those given by the above relations. The light ion drift amplitudes are $V_{xi} \sim 0.25\ a_{eo}$ and $V_{yi}=0.047\ a_{eo}$. For the electrons, the amplitudes are $V_{xe}= 0.25\ a_{eo}$ and $V_{ye} \sim 0$. As found before, mainly the heavy and light ion coupling due to the relative polarization drift, $V_{yrel}= V_{yh}-V_{yi} \approx 0.2\ a_{eo} \approx 4a_{io}$, drives the instability to generate the fluctuation in ϕ(t) plotted in Figure 2a.

Figure 2b shows that until t=23Ω_{ci}, $T_{\perp h}$ and $T_{\perp i}$ increase more or less smoothly, then there are two sudden jumps in $T_{\perp h,}$ separated by one driving field wave period τ_d. The step increases in the temperature coincide with bursts of large amplitude lower hybrid waves (Figure 2a). The frequency spectrum of the data plotted in Figure 2a is shown in Figure 2d. The noteworthy feature of the spectrum is the peak appearing near the lower hybrid frequency ω_{lh} ~13.6Ω_i; the lower hybrid frequency is given by

$$\omega_{lh} = \omega_{pi}[n_i + (n_h/4)]^{1/2} \times (1+\omega_{pe}^2/\Omega_e^2)]^{-1/2}, \qquad (4)$$

where ω_{pi} is the light ion plasma frequency with the total density $n_o=n_h+n_i$ and it is ω_{pi}~20Ω_i for M_i/m=400. Since Ω_e/ω_{pe}=1, n_{ih} = 0.1n_o and n_i=0.9n_o, we have ω_{lh}= 13.6Ω_i. We point out that even though the spectrum has a peak at ω_{lh}, it is quite broadband extending even below the heavy ion cyclotron frequency. The low-frequency behavior of the spectrum is perhaps an artifact of the adiabatic start in which the driving wave grows over several ion cyclotron periods. But the reason for wave power between the heavy ion cyclotron frequency and ω_{lh} is the generation of waves by the drifts shown in Figure 2c.

We point out that the LH waves are driven by the interaction of the slow-beam mode of the heavy ions and the Bernstein mode of the light ions [Seiler at al., 1976]. For such interactions the ion-ion instability growth rate maximizes near the light ion cyclotron harmonic just below the lower hybrid frequency, i.e., ω_{lh}~nΩ_i; in R-1 discussed here n=13. Seiler et al. [1976] studied this ion-ion interaction by linear instability analysis as well by laboratory experiment. The same ion-ion interaction mechanism operates when pick-up ions interact with the background plasma generating LH waves [Cairns and Gurnett, 1990; Singh, 2000]. Both heavy and light ions diffuse in velocity space under the influence of this instability affecting their heating. It is worth noting

that for such 'high-frequency' ion-ion interactions the heavy ions behave as un-magnetized ions because the interaction time is much shorter than the heavy ion cyclotron period. When the LH waves dominate the heating occurs primary by Landau resonance $\omega \sim k_y V_i$, where k_y is the perpendicular wave number and V_i is the ion velocity.

We performed runs R-2 and R-3 with driving wave frequencies ω/Ω_i =0.5, and 0.8, respectively. Figure 3 shows the comparison of the ion heating in the three runs R-1 to R-3. The top panels show the V_x-V_y phase space of light (black dots) and heavy (red dots) ions at initial time t=0. The middle panels show the same phase space at the end of the simulations (t=65.62 Ω_{ci}). *A noteworthy feature of the phase space in the middle panels is that they are not centered at $V_x=V_y=0$; they are off-centered due to the combined effects of E×B and polarization drifts.* The bottom panels show the evolution of the heavy and light ions' perpendicular temperatures, like in Figure 2b. The frequencies of the driving waves are labeled in the top panels. It is interesting to note that for the same amplitude, the driving wave becomes more effective in heating the ions as the wave frequency moves closer to the light ion cyclotron frequency. It is seen from the much larger spread of the phase space for ω/Ω_i =0.8 than that for ω/Ω_i =0.1875 and 0.5. We also see that heating rates for ω/Ω_i =0.8 are much larger than that for ω/Ω_i =0.1875 and 0.5.

The reason for the relatively large heating rate as ω tends toward the light ion cyclotron is the reduction in the drifts of heavy ions and the increase in the light ions drifts due to the resonance effects determined by the factor $(1-\omega^2/\Omega_s^2)^{-1}$ in (2) and (3). Figure 4 shows the evolution of the drift of both light and heavy ions as well as of electrons from R-3, in which ω=0.8Ω_i. The solid and dotted lines show the E×B and the polarization drifts respectively. The E×B drift for the heavy ions is $V_{xh} = 0.024 a_{eo}$, while for the light ions it is V_{xi}= 0.7 a_{eo} giving a relative drift

$V_{x,re1}= 0.72a_{eo}$. Note that the individual E×B drifts are out of phase, so they add to yield the relative velocity. The polarization drifts are $V_{yh}=0.09\ a_{eo}$ and $V_{yi}=0.55\ a_{eo}$, resulting into a relative drift $V_{y,re1}=0.63\ a_{eo}$. Note that $V_{x,re1}$ is slightly larger than $V_{y,re1}$.

Now let us consider the drifts if we had taken $\omega=0.8\omega_h$, below the heavy ion cyclotron frequency, the in-phase E×B drift of heavy and light ions are $V_{xh}= 0.7\ a_{eo}$ and $V_{xi}= 0.25\ a_{eo}$, respectively, yielding a relative drift $V_{x,\ rel2}$~$0.45\ a_{eo}$, which is much smaller than the above estimate of $V_{x,\ re1}$. The polarization drift of heavy and light ions are $V_{yh}= 0.55\ a_{eo}$ and $V_{yi}= 0.05\ a_{eo}$, yielding a relative drift $V_{y,\ rel2} =0.5\ a_{eo}$, which is also smaller than the $V_{y,\ re1}$ calculated above. Thus we learn that the resonance effect, in combination with the drifts of heavy and light ions being out-of-phase as the driving wave frequency increases above the heavy ion cyclotron frequency, produces much larger relative drifts between the light and heavy ion species than that for frequency being below the heavy ion cyclotron frequency. The larger the relative drift, the larger becomes the amplitude of the driven electrostatic waves and the resulting ion heating. This might explain the observation from Freja that the transverse ion heating correlates better with the EMIC waves above the He^+ cyclotron frequency than that with the waves below the O^+ cyclotron frequency as reported by Erlandson et al. [1994].

Figure 5a shows the evolution of the noise in the electric potential from R-3 as in Figure 2a for R-1. The wave amplitude in Figure 5a is generally larger than that in Figure 2a. Figure 2b shows the temporal behavior of the waves on an expanded time scale revealing that they contain strong features at light ion cyclotron period and the periods corresponding to higher cyclotron harmonics. The frequency spectrum of the noise in Figure 5a is plotted in Figure 5c. Comparing the spectra in Figure 2d and Figure 5c, we find that in the latter case the peak at the lower hybrid

(LH) frequency is washed out and the spectrum is nearly flat from a low frequency near the heavy ion cyclotron frequency ($0.25\Omega_i$) to the LH frequency, ω_{lh}~$13.6\Omega_i$. Furthermore, the power in the flat part of the spectrum in Figure 5c is about one order of magnitude larger than that in Figure 2d. A detailed examination of the waveforms in Figure 5a reveals that the noise consists of ion cyclotron oscillations at light and heavy ions' cyclotron frequencies as well as high frequencies extending up to the LH frequency. We learn from this simulation that EMELF wave electric fields near the light ion cyclotron frequency belonging to EMIC waves (Erlandson et al, 1994] as well as BBELF [Wahlund et al., 1998] waves could potentially generate broadband electrostatic turbulence.

3.2. Broadband Spectrum of the Driving Wave

In the above discussion we have examined the heating by monochromatic driving waves. However, observations reveal that BBELF waves are generally broadband extending in frequency from below the heaviest ion cyclotron frequency to above the light ion cyclotron frequency. Such waves at different frequencies might not be correlated either in time or space. The amplitude of such waves generally decreases with the increasing frequency, with exceptions of some peaks in the power spectrum. We model such waves as superposition of a large number of frequency components with random phase and amplitudes as follows:

$$E_y(t) = F_a(t)\, G(t), \qquad (5a)$$

$$G(t) = \sum_{j=1}^{N} A_j \sin(\omega_j t + \phi_j), \qquad (5b)$$

$$A_j = A_1 (\omega_1/\omega_j)^{\alpha}, \quad \phi_j = R_j\, 2\pi, \qquad (5c)$$

where the exponent α=1 in R-4, α=2 in R-5 and α=1/2 in R-6. The phase ϕ_j is uniformly distributed between zero and 2π determined by the random number R_j uniformly distributed over

$0<R_j<1$. $F_a(t)$ is the adiabatic start function defined earlier. N is the number of mono-chromatic waves in the broadband spectrum. We have used $A_1 = 0.25$, and $\omega_1 = 0.1\omega_i$. The separation between the consecutive frequencies is $\omega_{j+1} - \omega_j = 0.011\omega_i$ with j ranging from one to N=100. Thus the amplitude of the component with the maximum frequency is $A_1/10=0.025$ in Figure 6a (R-4) and $A_1/100=0.0025$ in Figure 8a (R=5). Figures 6a and 8a show G(t) for $\alpha=1$ and $\alpha=2$, respectively. We notice from Figures 6a and 8a that the superposition of several sinusoids with random phase produces impulsive electric field behavior. The impulses have large amplitudes several times the largest amplitude A_1. The smaller the exponent α the narrower and larger the impulses become. For _ =1/2, the impulses become unrealistically large and we do not discuss any results from R-6. How do the impulses affect the generation of electrostatic wave and associated ion heating?

Figure 6b shows the time history of the electric potential at the point (64, 64), like in Figure 2a from R-1. Figure 6c shows the corresponding evolution of the heavy and light ions perpendicular temperatures in the same format as in Figure 2b. Note that coinciding with the burst of electric noise (Figure 6b) near $t\sim6\text{-}7\omega_{ci}$ the perpendicular temperatures $T_{\perp h}$ and $T_{\perp i}$ rise sharply; the heavy ions' temperature $T_{\perp h}$ rises to $\sim45T_o$, while for the light ions the increase is to $T_{\perp i} = 15T_o$. After the sudden jumps in the temperatures the heating is relatively slow. The light ions heat with a nearly constant heating rate. The heavy ions heat discontinuously over a certain time range, but the jumps in the temperatures are relatively small. The sharp rise in temperatures near $t\sim6\text{-}7\omega_{ci}$ coincides with an impulse in the same time frame marked in Figure 6a by I_1. The small jumps in the heavy ion temperature in the time frame $t\sim14\text{-}20\omega_{ci}$ are associated with weaker bursts of noise seen in Figure 6b. When the ions are heated, the noise bursts becomes relatively

weak too as expected from theoretical considerations; the threshold criterion on the relative drifts are not met after the heating of the ions [Singh and Khazanov, 2004]. It is noteworthy that the large-amplitude impulses in $E_y(t)$ in the time frame from $t > 30\Omega_{ci}$ (Figure 6a) do not affect further heating of the heavy ions while the heating of the light ions continues. This is attributed to the fact that preferentially heated heavy ions have large Larmor radii and the ES waves heating them have comparable wavelengths. Thus the heating saturates for the heavy ions, while for the light ions with smaller Larmor radii the heating continues slowly till the end of the simulation.

Figure 6d shows the frequency spectrum of the electric potential plotted in Figure 6b. Note that the electrical noise becomes broadband extending up to the lower hybrid frequency $\omega_{lh} = 13.6\Omega_i$. The spectrum contains peaks near the heavy ion cyclotron frequency and its harmonics. Comparing the spectra in Figure 2d from R-1 and in Figure 6d, we find that the amplitude level at the frequencies below $10\Omega_i < \omega_{lh}$ is enhanced by an order of magnitude in R-4. Furthermore, the spectrum has become flatter.

In order to understand the origin of the large amplitude burst near $t\sim6\text{-}7\Omega_{ci}$, we examine the drift velocities of the light and heavy ions in this time frame. Figures 7a-7b show V_x (ExB drift V_d) and V_y (polarization drift V_d) for the light and heavy ions, respectively. The differences (V_{xi}-V_{xh}) and (V_{yi}-V_{yh}), giving the relative drifts in the x and y directions between light and heavy ions, are plotted in Figure 7c and 7d, respectively. Note the largest relative drifts occur for the first time in the period $t\sim6\text{-}7\Omega_{ci}$. The drifts coincide with the impulse I_1 in Figure 6a; the relative drifts caused by ExB drift and polarization drifts are nearly of equal magnitude $\sim 0.8\, a_{eo} \sim 16\, a_{io}$. Such drifts are large, but occur over a duration shorter than the ion cyclotron period, and produce

large-amplitude bursts of electrostatic noise. At latter times even larger drifts appear (not shown), but they do not generate similar large amplitude burst as in the time period t~6-7ω_{ci}. The reason for this is that the ions heated in the earliest event of the large-amplitude burst require an even larger drift for further wave generation [Singh and Khazanov, 2004].

Like in Figure 6a-6d for R-4, Figure 8 shows the time history of (a) $E_y(t)$ for β=2 as already mentioned, (b) electric potential ϕ(64,64), (c) ions' perpendicular temperatures and (d) the frequency spectrum of ϕ(64,64) from R-5. The frequency components of the driving field $E_y(t)$ in R-5 decay faster with the increasing frequency than that in R-4. This results into smaller amplitude of the impulses in $E_y(t)$ as seen in Figure 8a. In turn, this results in smaller amplitude bursts and at a later time in R-5 than that in R-4. The ion heating shows the steps in the perpendicular heating of both heavy and light ions near t~20ω_{ci} (Figure 8c) , but the step sizes in $T_{\perp h}$ and $T_{\perp i}$ are relatively smaller in R-5 than that in R-4. Each burst in ϕ(t) is associated with a clearly visible step in heating of the heavy ions over the interval t~20-30ω_{ci}. The frequency spectrum in Figure 8d shows the LH peak and additional peaks below the LH frequency.

The appearance of the LH peak in Figure 8d and its absence in Figures 6d and in Figure 5c have the following physical implication. When a high frequency EMELF wave dominates the frequency spectrum of the BBELF waves, the drift generated ES waves tend to have flatter spectrum than that for the EMELF spectrum being dominated by the low frequency waves.

4. Conclusions and Discussions

Our main conclusions are the following.

a. When an EMELF wave permeates a plasma, the drifts of the charged particles in the transverse electric field of the wave generate electrostatic waves, which heat the ions transversely.
b. The frequencies of the generated electrostatic waves range over the ion cyclotron harmonics to lower hybrid frequency, appearing as broadband electrostatic noise.
c. When EMELF waves constitute a broad spectrum including electromagnetic ion cyclotron waves ranging in frequency from below the heavy ion cyclotron frequency up to the light ion cyclotron frequency, their superposition produces impulsive electric fields of large amplitudes in time domain.
d. The drifts in the large-amplitude impulses produce a burst of large-amplitude electrostatic noise, which causes sudden perpendicular heating of both heavy and light ions. For the heavy ions several events of such step heating occur while the light ions undergo a smooth heating after the first step.
e. For the amplitudes of the waves considered here, the perpendicular heating is significant. The ions can be heated up to several tens of the initial ion temperature.
f. For the EMIC waves, the waves having frequencies between the light and heavy ions are more effective in transverse ion heating due the larger relative drifts between the different ion species due to the 180 phase difference between the drifts of the individual species. This phase difference comes from the resonance factor $1/(1-\square^2/\square_{\_}^2)$; for heavy ions this factor is negative while it is positive for the light ions.
g. The flatness of the generated ES wave spectrum depends on the dominance of the high frequency component of the EMELF (Alfvénic) waves.

Our simulations, as discussed here, demonstrate that EMELF, including electromagnetic ion cyclotron waves, can be dissipated via the generation of electrostatic waves produced by the relative drift between ions of different species by the former waves. A direct application of our results presented here is the observation of broadband extremely low frequency waves (BBELF) and associated ion heating. BBELF waves have been observed in rocket experiments [Boehm et al., 1990], and from several satellites such as Freja [Louarn et al., 1994], FAST [Stasiewicz et al., 2000; Chaston et al, 2004] and Cluster [Wahlund et al., 2003]. However, it is now well established that EMELF waves are invariably associated with high-frequency electrostatic waves extending in frequency up to the lower hybrid frequency, which is close to the H^+ plasma frequency. These assertions are highlighted by the Cluster observation of BBELF waves reported by Wahlund et al. [2003] and more recently by Klatt et al. [2005] based on SIERRA observations. As presented by Wahlund et al. [2003], the Cluster data reveals the following properties of BBELF. The observations were made at a high altitude of 4-5 R_e. The frequency spectrum of both EMELF and electrostatic components are plotted in Figure 1 up to 10 Hz and as mentioned by Wahlund et al., it continues with enhanced power level up to 300-400 Hz, which is about the H^+- plasma frequency f_{ph} =370 Hz. The other characteristic frequencies in the plasma for the Cluster observations are proton cyclotron f_{ci}~7.5 Hz, electron plasma frequency f_{pe}~15 kHz, and electron cyclotron frequency f_{ce}~14 kHz. For these parameters the lower hybrid frequency is f_{lh}~260 Hz, close to the approximate upper frequency limit of the electrostatic component of the BBELF waves. Klatt et al. [2005] shows that peaks in the burst of electrostatic waves extend to the LH frequency and beyond it as VLF waves. They interpret their results to the presence of lower-hybrid solitary structures (LHSS) [LaBelle et al., 1986; Kintner et al., 1992; Vago et al., 1992; Lynch et al., 1999; Schuck et al., 2003].

Despite a large number of studies on LHSS, the energy source for the LHSS remains undetermined. A myriad of electrodynamic processes consisting of Alfvén waves solitary structures, transverse ion heating, formation of density cavities, large parallel electric fields in the cavities, field-aligned burst of electrons, transversely limited wave packets of lower hybrid waves in cavities (LHSS), and all on the same auroral field lines have been observed. It is established now that the transverse heating of ions is caused by Alfvén waves as well as lower hybrid waves [Andre et al., 1998; Lynch et al., 1999]. It is also demonstrated by modeling that density cavities are a natural consequence of transverse heating of ions [Singh, 1992; Singh and Chan, 1993; Singh, 1994,1996]. Connection between density cavities and parallel electric fields in the cavities in association with Alfvén waves are established by both observations [Chaston et al., 2006] and modeling of current-cavity interaction [Singh, 2002; Singh, 2005]. The parallel electric fields in the form of a double layer in the cavity create an electron beam. The lower hybrid waves can be generated by the Alfvén waves directly as studied in this paper as well as by the electron beam, especially if the beam is thin in the transverse direction [Singh et al., 1985; 2001]. *However, the knowledge of the electrodynamic processes mentioned here exists only in piecemeal.* A self-consistent kinetic modeling at meso-scale size is needed to establish the mutual coupling between them. Such a study is likely to reveal the source of energy for the LHSS events.

For the EMELF waves at frequencies below the heavy ion cyclotron frequency the polarization drift of heavy ions, V_{yh} a given by (3), drives the instability. This drift depends on the frequency via the factor $H(\Omega) = \Omega/(1- \Omega^2)$ where $\Omega = \omega/\omega_h$. For $\Omega<0.6$, the factor $H(\Omega)$ reduces the drift rapidly as the frequency decreases. On the other hand, for $\Omega>0.6$ this factor increases rapidly as the frequency increases toward the heavy ion cyclotron frequency. Thus the

latter range of the frequency spectrum of the EMELF waves have the potential for driving strong instabilities and ion heating depending on the perpendicular electric field because $V_{yh} \sim E_{\perp} / B_o$. Since EMELF waves have very small parallel wave numbers they are difficult to have cyclotron resonance with thermal ions, especially at low altitudes of Freja and FAST where characteristic ion energy is ~0.15 eV. The EMELF waves in the frequency range $0.6 < \omega/\omega_h < 1$ are likely to drive the instabilities studied in this paper and heat the cold ions even when they are not directly in cyclotron resonance with the waves. Our study shows that if the waves are broadband, the resulting time-domain impulses in $E_{\perp}$ have large amplitudes, resulting in larger drifts and heating of ions (Figures 7 and 8).

We give some estimates here of the heating based on wave amplitudes and frequencies observed from Freja, FAST and Cluster. Since the polarization drift scales as $V_{yh} \sim H(\omega)\ (E_{\perp} / B_o)$, and instability threshold is $V_{yh} \sim a_i$, the light ion evolving thermal velocity [Khazanov et al., 1997a], the extent of light ion heating scales as $T_{\perp i} \sim 0.5\ M_i\ H(\omega)^2\ (E_{\perp} / B_o)^2$ [Singh and Khazanov, 2004]. Heavy ions heat somewhat higher. For the Cluster data in Figure 1, $E_{\perp} \sim 100$ mV/m and $B_o \sim 160$ nT, giving an estimate of the heating $T_{\perp i} \sim 0.5\ H(\omega)^2\ M\ (E_{\perp} / B_o)^2 \sim 3.5$ keV with $\omega \sim 0.7$. At the altitudes covering Freja and FAST, we have $E_{\perp} \sim$ 25-1000 mV/m and $B_o \sim$12,000-25,000 nT. Specifically, we take the example from Figure 1 of Andre et al. [1998]; In this case B~25,000 nT and $E_{\perp} \sim$ 200-600 mV/m, giving V_{yh} ~10-30 km/s for $\omega \sim 0.7$. For such drifts light ion heating is estimated as 1-10 eV. If we choose a higher frequency, the heating estimate is increased; for $\omega \sim 0.9$, we have an increase by a factor of ~20 giving the estimate ~20-200 eV. Ion heating within the ballpark of this estimate is reported by Andre et al. [1998]. This increase is simply accounted for by the increase in $H(\omega)^2$. Chaston et al. [2004] also report temperatures of ions observed with Alfvén waves in this ballpark using FAST data. Knudsen and

Wahlund [1998] reported micro-bursts of core ions heated to a few eV associated with EMELF waves with low amplitudes ~25 mV/m. Even for such low amplitudes, the polarization drift of heavy ions can be sufficiently high to excite instabilities in H^+- O^+ plasma and heat the ions; For example, if Ω ~0.9 the drift V_{yh}~ 5 km/s reaching the thermal velocity of 0.15-eV H^+ ions. Heavy ions are expected to heat ~2.5 eV in such instabilities. As pointed out earlier, if the waves are broadband, the resulting time-domain electric field impulses have large amplitudes and affect stronger heating compared to the estimates given here for the monochromatic waves. The heating by the instability mechanism does not require direct ion cyclotron resonance with the EMELF waves.

The heating by ion cyclotron resonance as proposed by Chang et al. [1986] and applied to Freja data runs into several difficulties. First of all Andre et al. [1998] point out that it takes only about **1%** of the observed wave power to achieve the measured level of heating. A question arises as to why the heating is so severely limited. The other difficulty is determination of the power spectral density (PSD) from the measurements. The critical PSD at the O^+ cyclotron frequency 25 Hz (~10^{-4} $m^2V^2/m^2/Hz$) for ion heating found from Freja is derived from time series measured during the traversal of the EMELF waves by the satellite [Knudsen et al., 1998]. It is not certain whether the satellite measured spatial or temporal features or their combinations [Stasiewicz et al., 2000; Chaston et al., 2004]. Thus the PSD values estimated from Freja measurements need to be reexamined and resulting ion heating reassessed.

It is important to point out that if ions are already hot having temperatures as estimated above, further heating by the instability mechanism is not operative. A direct consequence of this finding is that ion heating might occur when the EMELF waves propagate down where ions are cooler. At very low altitudes, where electron skin depth and ion Larmor radii become

comparable, the EMELF waves might directly heat the ions by demagnetizing them as suggested by Cole [1976] and seen in numerical simulations of V-shaped double layers [Borovsky, 1984; Greenspan, 1984; Singh et al., 1987; Singh and Khazanov, 2003] and in heating of ions by narrow scale shear Alfvén waves [Stasiewicz et al., 2000; Chaston et al., 2004].

We point out that for a quantitative one-to-one comparison between the features of EMELF waves, their continuation to high frequencies as electrostatic waves and associated ion heating as seen in satellite and rocket observations and simulations, the latter needs to be performed with specific plasma conditions of the observations and real masses of ion species. We also need to include in the simulations the finite perpendicular wavelengths of the EMELF waves. We plan to do this in the near future. The work in this paper is meant to reveal the basic physical processes involved in generation of the electrostatic waves and resulting ion heating when the plasma is driven by a single monochromatic EMELF wave or a broad spectrum of them.

Acknowledgement: This work was supported by NASA grant NAG513489 and a grant from Marshall Space Flight Center.

References

André, M., P. Norqvist, L. Andersson, L. Eliasson, A. I. Eriksson, L. Blomberg, R. E. Erlandson, and J. Waldemark, Ion energization mechanisms at 1700 km in the auroral region, *J. Geophys. Res.*, *103*(A3), 4199–4222, 1998.

Angelopoulos, V., J. A. Chapman, F. S. Mozer,1 J. D. Scudder, C. T. Russell, K. Tsuruda, T. Mukai, T. J. Hughes, and K. Yumoto, Plasma sheet electromagnetic power generation and its dissipation along auroral field lines, *J. Geophys. Res.,* 107, NO. A8, 1181, 10.1029/2001JA900136, 2002.

Birdsall, C. K., and A. B. Langdon, *Plasma Physics Via Computer Simulation*, Chap. 14, pp. 305-350, McGraw-Hill, New York, 1985.

Boehm, M. H., W. Carlson, J. P. McFadden, J.H. Clemmons, and F.S. Mozer, High-resolution sounding rocket observations of large-amplitude Alfvén waves, *J. Geophys, Res. 95*, 5877, 1990.

Bonnell, J., P. M. Kintner, J.E. Wahlund, K. Lynch and R. Arnoldy. Interferometric determination of broadband ELF wave phase velocity within a region of transverse auroral ion acceleration, *Geophys. Res. Lett., 23,* 3297, 1996.

Borovsky, J. E., The production of ion conics by oblique double layers, *J. Geophys, Res. 89*, 2251, 1984.

Cairns, I. H., and D. A. Gurnett, Control of plasma waves associated with the space shuttle by the angle between the orbit's velocity vector and the magnetic field, J. Geophys. Res., 96, 751, 1990.

Chaston, C.C., J.W. Bonnell, C.W. Carlson, J.P. McFadden, R.E. Ergun, R.J. Strangeway, and E.J. Lund, Auroral ion acceleration in dispersive Alfvén waves, *J. Geophys, Res. 109,* A04205, 2004.

Chust, T., P. Louarn, M. Volwerk, H. de Feraudy, A. Roux, J. Wahlund, and B. Holback, Electric fields with a large parallel component observed by the Freja spacecraft: Artifacts or real signals?, *J. Geophys. Res.*, *103*(A1), 215–224, 1998.

Cole, K. D., Effects of crossed magnetic and (spatially dependent) electric fields on charged particle motion, *Planet Space Sci., 24*, 515, 1976.

Erlandson, R.E., L.J. Zanetti, M.H. Acuña, A.I. Eriksson, L. Eliasson, M.H. Boehm, and L.G. Blomberg, Freja observations of electromagnetic ion cyclotron ELF waves and transverse oxygen ion acceleration on auroral field lines, *Geophys. Res. Lett., 21,* 1855, 1994.

Greenspan, M.E., Effects of oblique double layers on upgoing pitch angle and gyrophase, *J. Geophys, Res., 89,* 2842, 1984.

Keiling, A., G.K. Parks, J.R. Wygant, J. Dombeck, F.S. Mozer, C.T. Russell, A.V. Streltsov, W. Lotko, Some properties of Alfvén waves: Observations in the tail lobes and the plasma sheet boundary layer, *J. Geophys. Res.,* Vol. 110, No. A10, A10S11, 2005.

Khazanov, G. V., E. N. Krivorutsky, T. E. Moore, M.W. Liemohn, and J.L. Horwitz, Lower hybrid oscillations in multicomponent space plasmas subjected to ion cyclotron waves, *J. Geophys. Res., 102* 175, 1997a.

Khazanov, G. V., M.W. Liemohn, E. N. Krivorutsky, and J.L. Horwitz, A model for lower hybrid wave excitation compared with observations by Viking, *Geophys. Res. Lett., 24,* 2399, 1997b.

Kintner, P.M., J. Bonnell, R. Arnoldy, K. Lynch, C. Pollock, and T. Moore, SCIFER – Transverse ion acceleration and plasma waves, comparison to Freja satellite observations, *Geophys, Res. Lett., Vol. 23*, 1873, 1996.

Kintner, P. M., J. Vago, S. Chesney, R. L. Arnoldy, K. A. Lynch, C. J.Pollock, and T. E. Moore,Localized lower hybrid acceleration of ionospheric plasma, Phys. Rev. Lett., 68(16), 2448–2451, 1992.

Klatt, E.M., P.M. Kintner, C.E. Seyler, K. Liu, E.A. MacDonald, and K.A. Lynch, SIERRA Observations of Alfvénic processes in the topside auroral ionosphere, *J. Geophys, Res. 101*, A10S12, 2005.

Knudsen, D. J., J. H. Clemmons, and J. Wahlund, Correlation between core ion energization, suprathermal electron bursts, and broadband ELF plasma waves, *J. Geophys. Res.*, *103*(A3), 4171–4186, 1998.

Knudsen, D. J., and J. Wahlund, Core ion flux bursts within solitary kinetic Alfvén waves, *J. Geophys. Res.*, *103*(A3), 4157–4170, 1998.

Labelle, J., P. M. Kintner, A. W. Yau, and B. A. Whalen, Large amplitude wave packets observed in the ionosphere in association with transverse ion acceleration, J. Geophys. Res., 91, 7113– 7118, 1986.

Louarn, P., J.E. Wahlund, T. Chust, H. de Feraudy, A. Roux, B. Holback, P.O. Dovner, A.I. Eriksson, and G. Holmgren, Observations of kinetic Alfvén waves by the Freja satellite, *Geophys. Res. Lett., 21,* 1847, 1994.

Lynch, K. A., R. L. Arnoldy, P. M. Kintner, P. Schuck, J. W. Bonnell, andV. Coffey, Auroral ion acceleration from lower hybrid solitary structures: A summary of sounding rocket observations, J. Geophys. Res., 104(A12), 28,515–28,534, 1999.

Schuck, P. W., and J. W. Bonnell, Ray trajectories of lower hybrid solitary structures, *J. Geophys. Res.*, *108*(A5), 1175, doi:10.1029/2002JA009716, 2003.

Seiler, S., M. Yamada, H. Ikezi, Lower hybrid instability by a spiraling ion beam, *Phys Rev. Lett., 37*, 700, 1976.

Seyler, C.E., and T. Xu, The relationship between field-aligned currents and low-frequency electromagnetic fluctuations, *Geophys. Res. Lett., Vol. 30,* 2106, 2003.

Singh, N., Plasma Perturbations Created by Transverse Ion Heating Events in the Magnetosphere, *J. Geophys. Res.*, *97*(A4), 4235–4249,1992.

Singh, N., Pondermotive versus mirror force in creation of thin filamentary cavities in auroral plasma, *Geophys. Res. Lett, 21*, 257, 1994.

Singh, N., Time Response of O^+ to a weak transverse ion heating event in the polar ionosphere, *J. Geophys. Res., 101,* A8, 5317-5328, 1996.

Singh, N., Cross-current instability generated by pick-up ions in the environment of a large spacecraft in low earth orbit, IEEE trans. Plasma Sci., 28, 2085-2096, 2000.

Singh, N., Spontaneous formation of current driven double layers in density depletions and its relevance to solitary Alfven waves, *Geophys. Res. Lett*., *29*, 51-1 – 51-4, April 2002.

Singh, N. Interrelation Among Double Layers, Parallel Electric Fields and Density Depletions, in Particle Acceleration in Astrophysical Plasmas, *Geophysical Monograph Series 156,* 10.1029/156GM25, p.231-247, 2005.

Singh, N., and C. B. Chan, Numerical simulation of plasma processes driven by transverse ion heating, *J. Geophys. Res.*, *98*(A7), 11,677–11,688, 1993.

Singh, N., J. R. Conrad and R.W. Schunk, Electrostatic ion-cyclotron, beam- plasma and lower hybrid waves excited by an electron beam, *J. Geophys. Res., 90*, 5l59, l985.

Singh, N., and W. C. Leung, Nonlinear features of electrostatic ion cyclotron instability driven by counterstreaming ion beams in equatorial outer plasmasphere, *J. Geophys. Res*., *104*, 28,547-558, 1999.

Singh, N, and Igor Khazanov, Dynamical Planar Double Layers: Filamentary Substructures, Electron Holes and Ion Heating, *Geophysical Research Letters, 30*, 2262, 2003.

Singh, N., G. Khazanov, Numerical simulation of waves driven by plasma currents generated by low-frequency Alfvén waves in a multi-ion plasma, *J. Geophys, Res. 109*, A05210, 2004.

Singh, N., S. M. Loo, B. Earl Wells, and G. S. Lahkina, Evolution of electron beam generated waves resulting into transverse ion heating and filamentation of the plasma, *J. Geophys. Res.*, *106,* 21165-21182, 2001.

Singh, N., H. Thiemann, and R.W. Schunk, Electric Fields and Double Layers in Plasmas, *Laser and Particle Beams, 5,* 233, l987.

Stasiewicz, K., R. Lundin, and G. Marklund, Stochastic ion heating by orbit chaotization on electrostatic waves and nonlinear structures, *Physica Scripta, Vol T84,* 60-63, 2000.

Vago, J. L., P. M. Kintner, S. W. Chesney, R. L. Arnoldy, K. A. Lynch, T. E.Moore, and C. J.Pollock, Transverse ion acceleration by localized lowerhybrid waves in the topside auroral ionosphere, J. Geophys. Res., 97,16,935– 16,957, 1992.

Wahlund, J.E.., et al., Observations of ion acoustic fluctuations in the auroral topside ionosphere by the FREJA S/C, *Geophys. Res. Lett., 21,*1835, 1994a.

Wahlund, J.E., P. Louarn, T. Chust, H. de Feraudy, A. Roux, B. Holback, P-O. Dovner, and G. Holmgren, On ion acoustic turbulence and the nonlinear evolution of kinetic Alfvén waves in aurora, *Geophys. Res. Lett., 21,* 1831, 1994b.

Wahlund, J.E., A.I. Eriksson, B. Holback, M. H. Boehm, J. Bonnell, P.M. Kintner, C.E. Seyler, J.H. Clemmons, L. Eliasson, D.J. Knudsen, P. Norqvist, and L. J. Zanetti, Broadband ELF plasma emission during auroral energization 1. Slow ion acoustic waves. *J. Geophys, Res. 103*, 4343, 1998.

Wahlund, J.E., A. Yilmaz, M. Backrud, D. Sundkvist, A. Vaivads, D. Winningham, M. André, A. Balogh, J. Bonnell, S. Buchert, T. Carozzi, N. Cornilleau, M. Dunlop, A.I. Eriksson, A. Fazakerley, G. Gustafsson, M. Parrot, P. Robert, and A. Tjulin, Observations of auroral broadband emissions by CLUSTER, *Geophys. Res. Lett., 30,* 1563, 2003.

Wygant, J. R., et al., Polar Spacecraft based comparisons of intense electric fields and Poynting flux near and within the plasma sheet-sheet boundary to UVI images: An energy source for the aurora, *J. Geophys. Res.,* 105, 18,675, 2000.

Wygant, J. R., et al., Evidence for kinetic Alfvén waves and parallel electron energization at 4-6 R_E altitudes in the plasma sheet boundary layer, *J. Geophys. Res.,* 107, A8, 1201, 10.1029/2001JA00113, 2002

----------IMPORTANT PUBLICATION INFORMATION----------

To ensure prompt publication:

Figure Captions:

Figure 1. Observed power spectrum of BBELF waves from Cluster [Wahlund et al., 2003]: (a) Power spectrum of electric field in quiet (bottom curve) and disturbed (top curve) regions traversed by Cluster. (b) Magnetic field spectra corresponding to the spectra in (a).

Figure 2. Temporal evolution of (a) electrostatic wave amplitude, (b) perpendicular ion temperatures of light and heavy ions, (c) Polarization (V_{yh}) and ExB (V_{xh}) drift velocities of heavy ions, and (d) frequency spectrum of the drift-driven electrostatic waves in (a) from R-1.

Figure 3. Comparison of transverse ion heating of light and heavy ions as seen from R-1 to R-3: top panels show the initial V_x-V_y phase space for the driving frequency labeled in the panels, middle panels show the same phase space at the end of the simulations at t=65.62Ω_{ci}. The bottom panels show the evolution of the perpendicular temperatures of heavy (solid line) and light (dotted line) ions.

Figure 4. Temporal evolution of the drifts of light ions (top panel), heavy ions (middle panel) and electrons (bottom panel) from R-3, in which Ω_d/Ω_i=0.8.

Figure 5. Temporal evolution: (a) electrostatic wave amplitude. (b) Same as (a) but over an expanded horizontal scale. (c) Frequency spectrum of data plotted in (a) from R-3.

Figure 6. Temporal evolution of (a) the driving electric field amplitude $E_y(t)$ for the power-law spectra with the exponent □=-1. (b) the wave amplitude, (c) perpendicular temperatures of heavy and light ions and (d) frequency spectrum of the data plotted in (b) from R-4.

Figure 7. Temporal evolution of the drifts of (a) light ions, (b)heavy ions (c) relative drifts between heavy and light ions due to their ExB drifts, (d) same as (c) but due to their polarization drifts, and ((e) drifts of electrons from R-4. The time period shown in these panels cover the large-amplitude burst of electrostatic noise in Figure 6a.

Figure 8. Same as Figure 6, but from R-5 in which the exponent in the power law spectrum is □=-2.

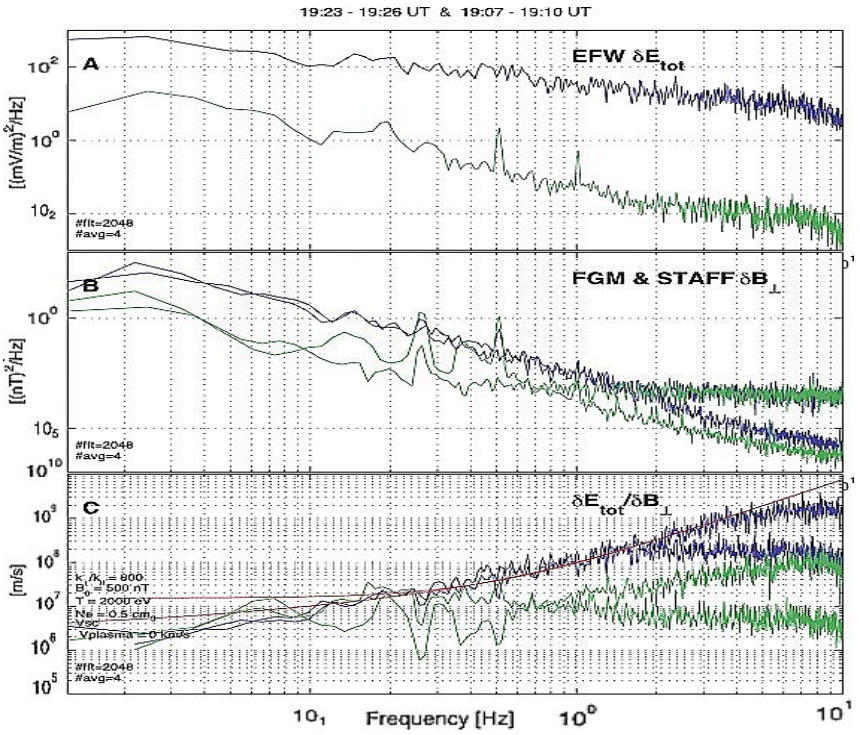

Figure 1. Observed power spectrum of BBELF waves from Cluster [Wahlund et al., 2003]: (a) Power spectrum of electric field in quiet (bottom curve) and disturbed (top curve) regions traversed by Cluster. (b) Magnetic field spectra corresponding to the spectra in (a).

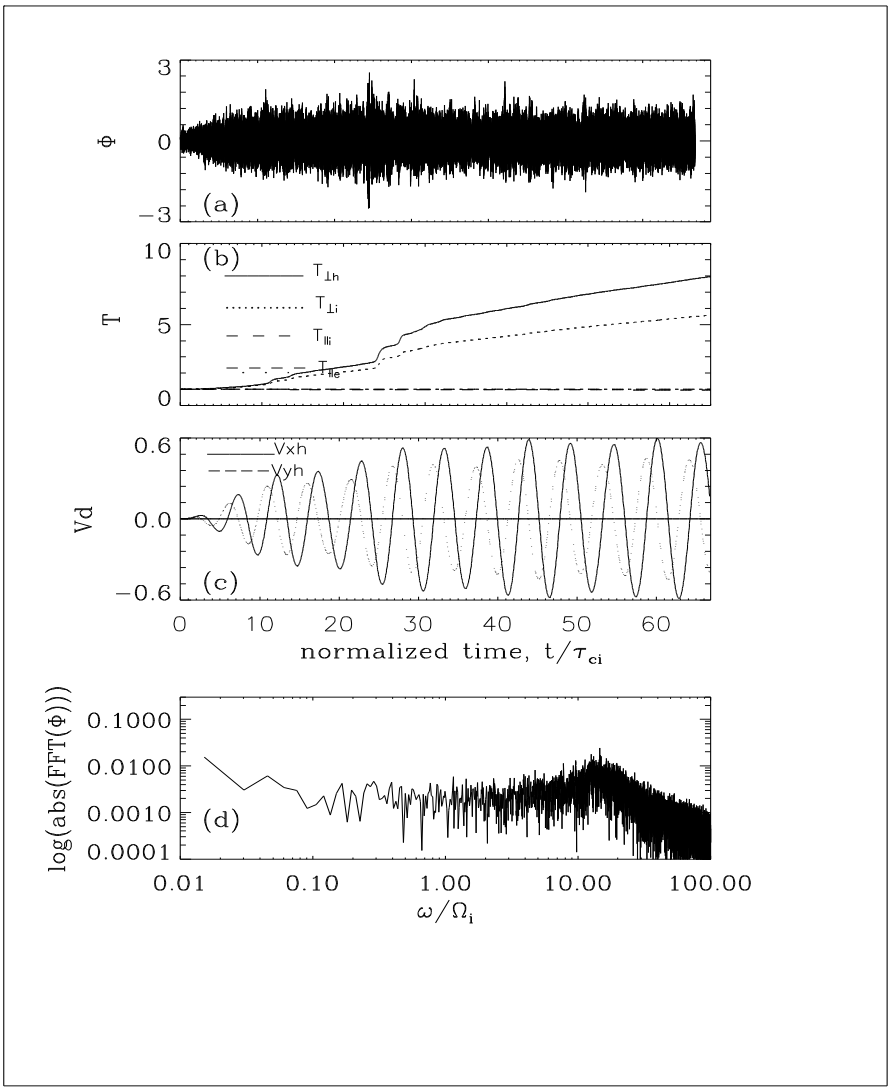

Figure 2. Temporal evolution of (a) electrostatic wave amplitude, (b) perpendicular ion temperatures of light and heavy ions, (c) Polarization (V_{yh}) and ExB (V_{xh}) drift velocities of heavy ions, and (d) frequency spectrum of the drift-driven electrostatic waves in (a) from R-1.

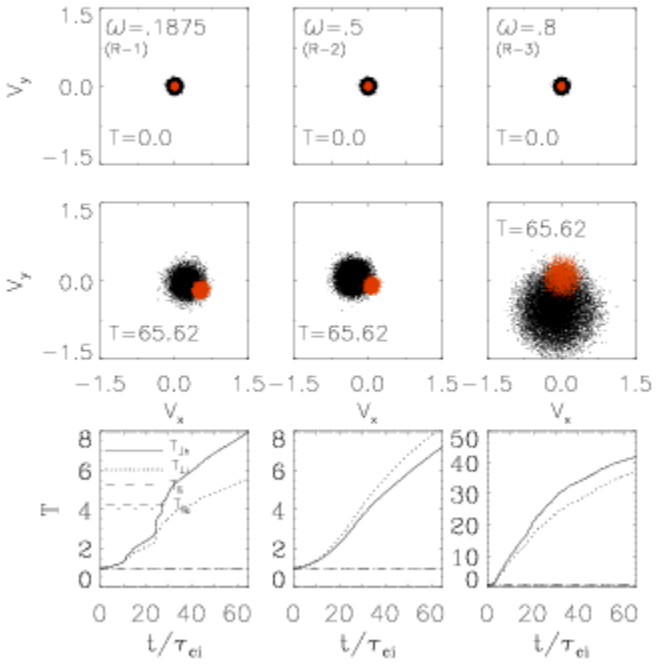

Figure 3. Comparison of transverse ion heating of light and heavy ions as seen from R-1 to R-3: top panels show the initial V_x-V_y phase space for the driving frequency labeled in the panels, middle panels show the same phase space at the end of the simulations at $t=65.62\tau_{ci}$. The bottom panels show the evolution of the perpendicular temperatures of heavy (solid line) and light (dotted line) ions.

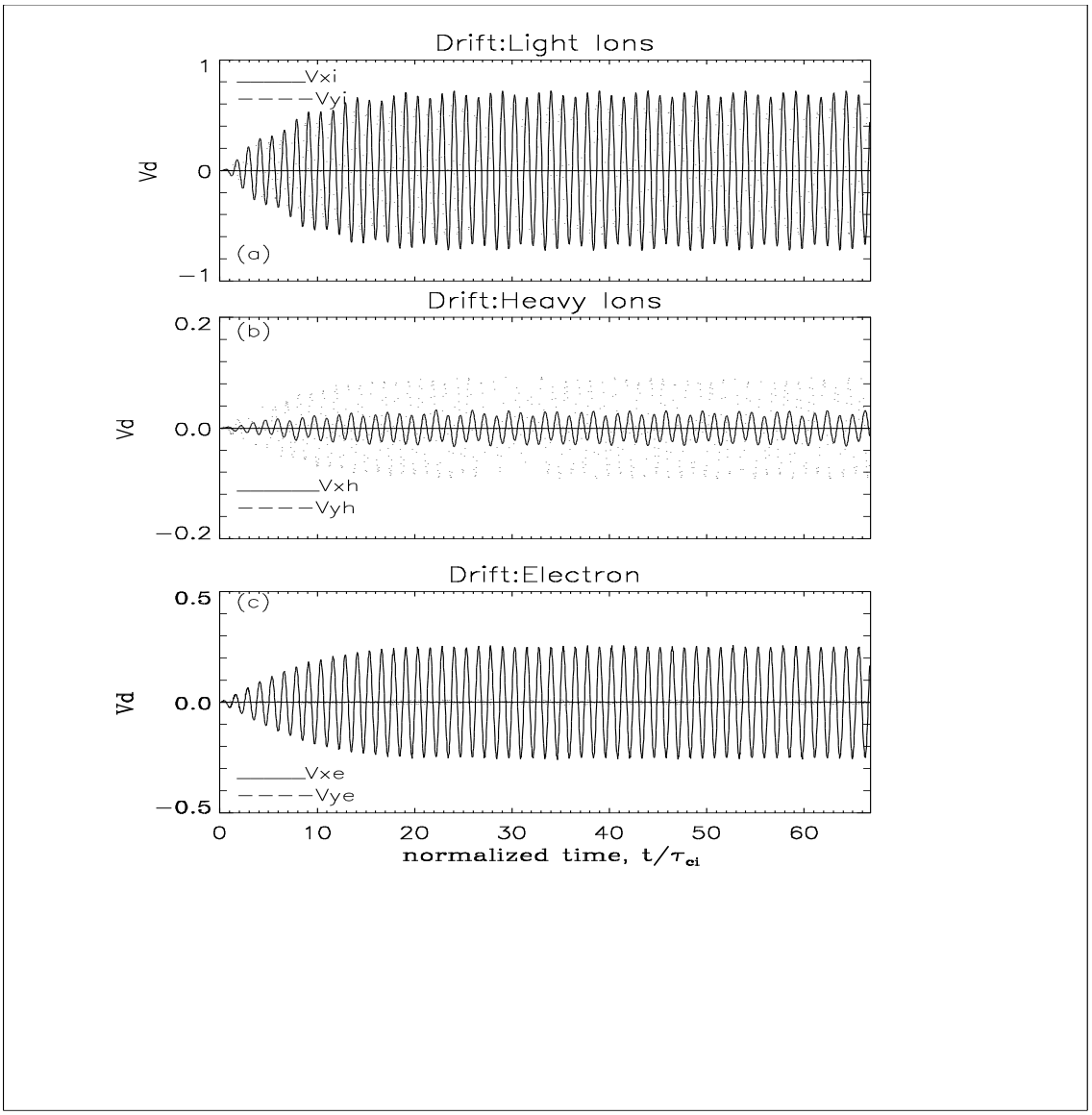

Figure 4. Temporal evolution of the drifts of light ions (top panel), heavy ions (middle panel) and electrons (bottom panel) from R-3, in which ρ_d/ρ_i=0.8.

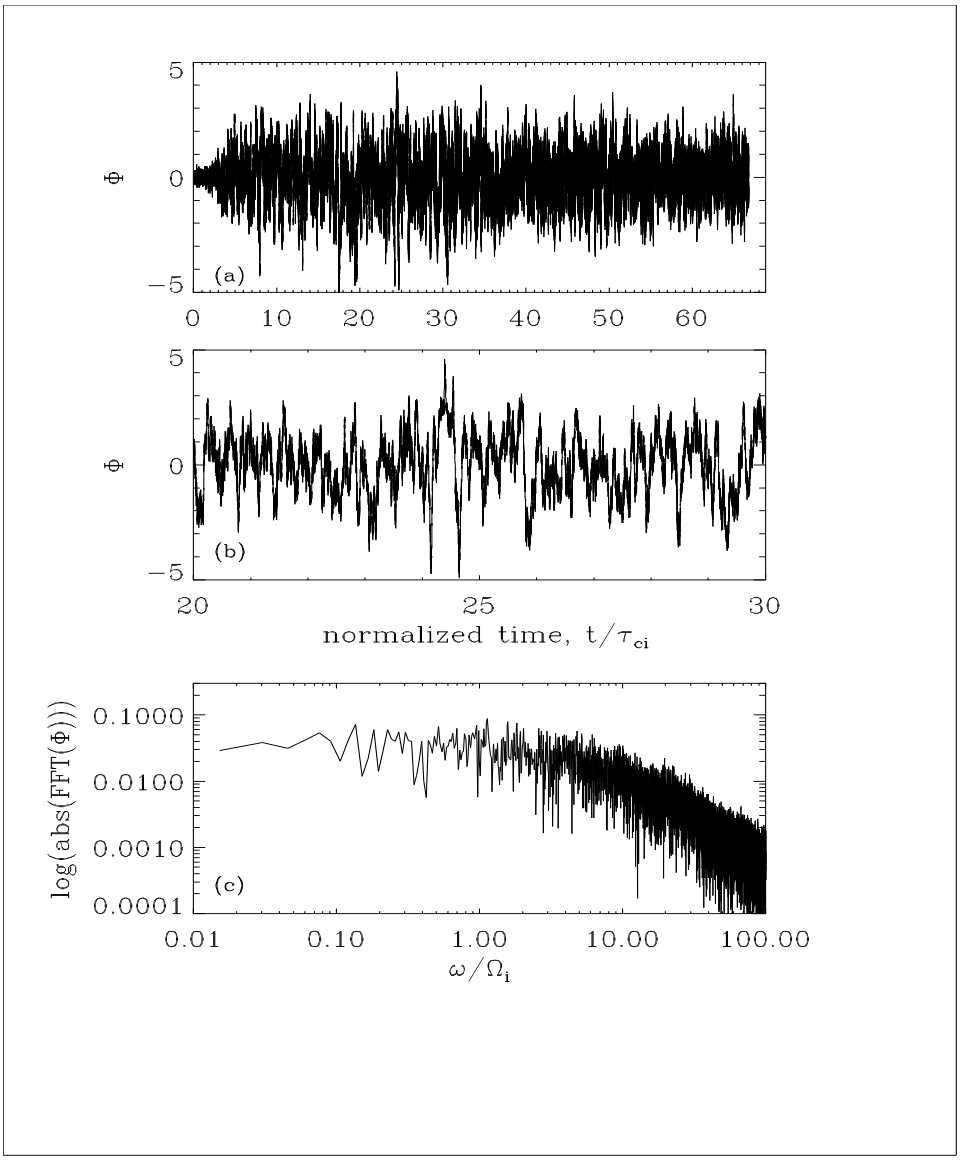

Figure 5. Temporal evolution: (a) electrostatic wave amplitude. (b) Same as (a) but over an expanded horizontal scale. (c) Frequency spectrum of data plotted in (a) from R-3.

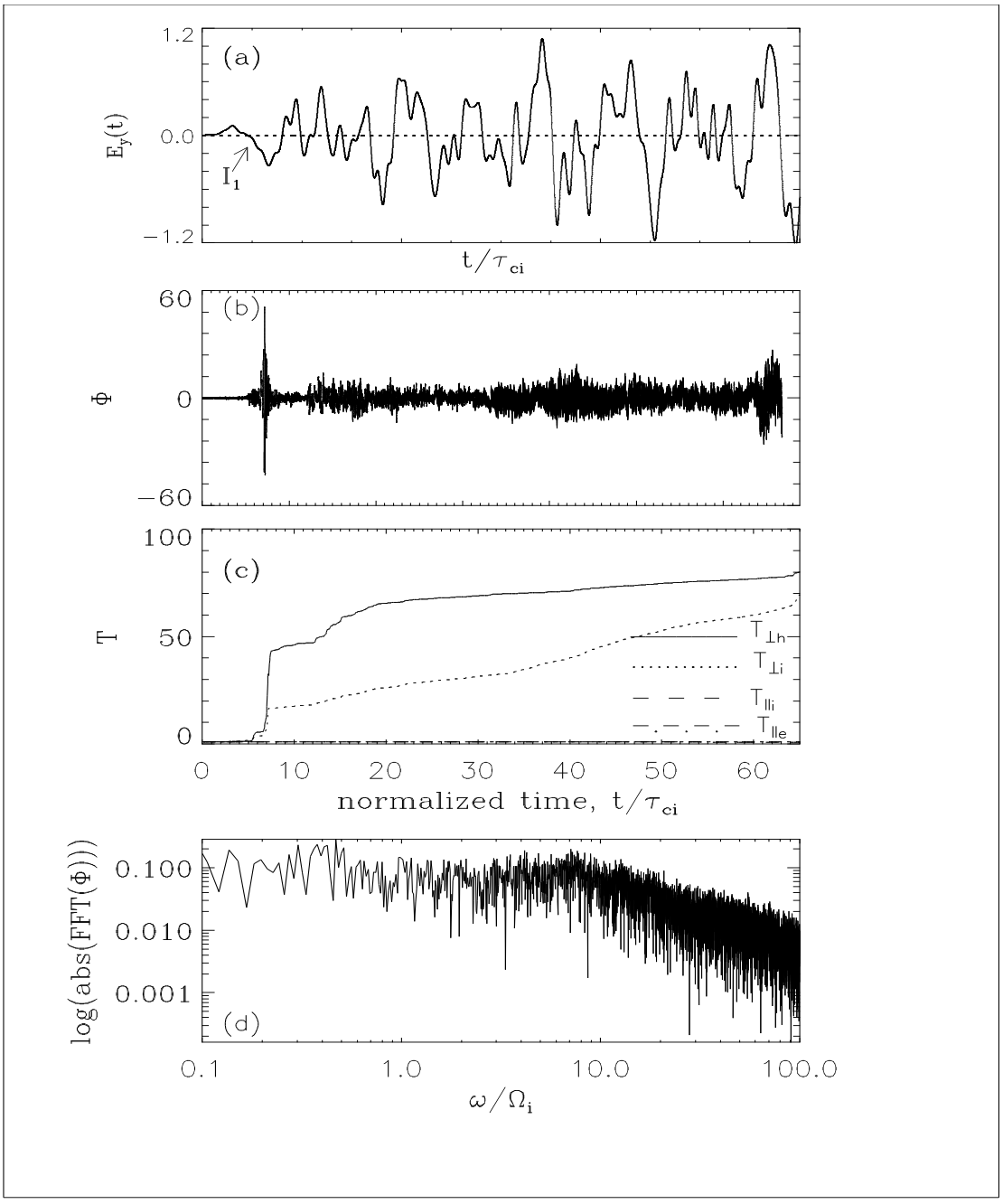

Figure 6. Temporal evolution of (a) the driving electric field amplitude $E_y(t)$ for the power-law spectra with the exponent □=-1. (b) the wave amplitude, (c) perpendicular temperatures of heavy and light ions and (d) frequency spectrum of the data plotted in (b) from R-4.

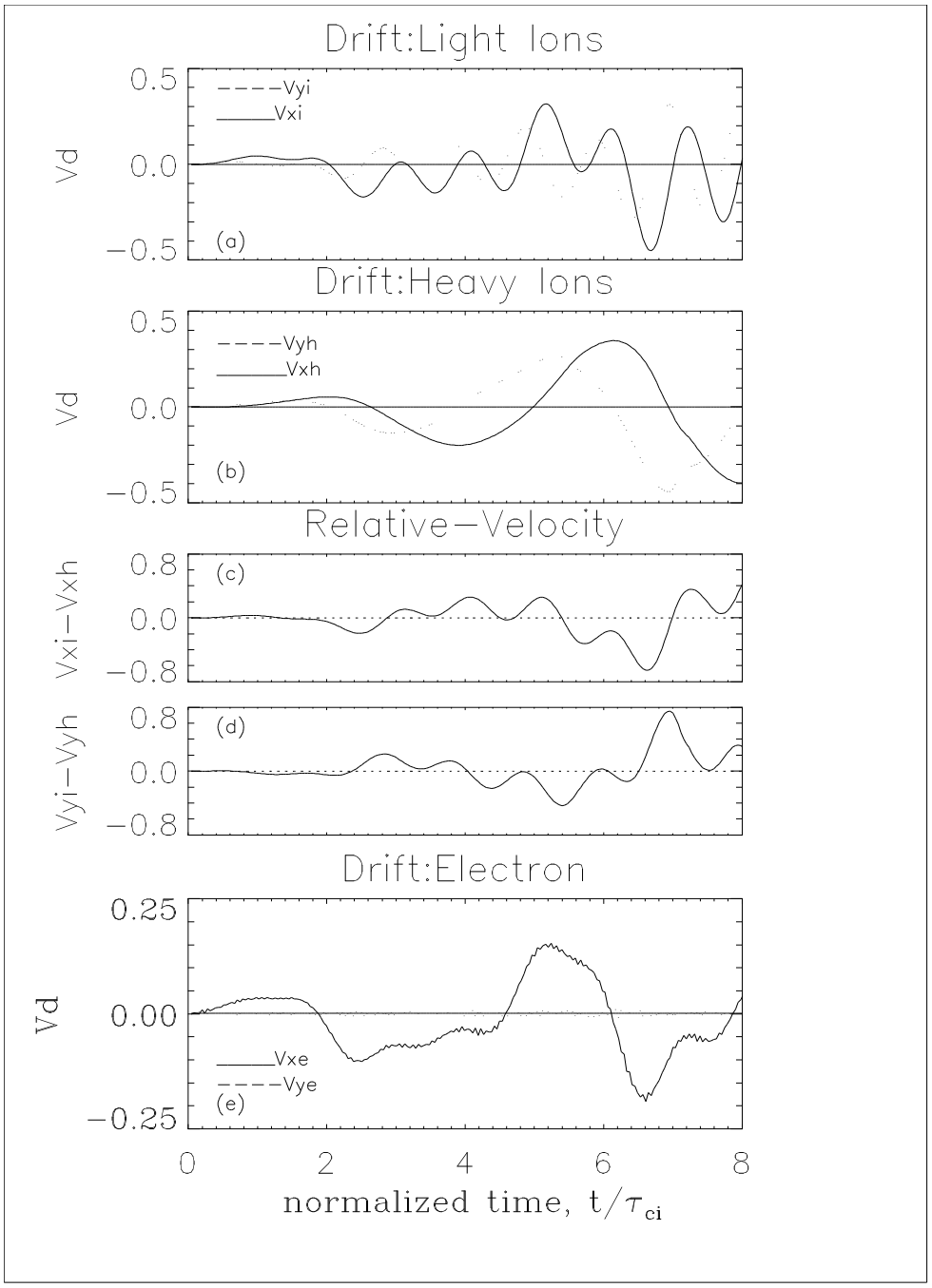

Figure 7. Temporal evolution of the drifts of (a) light ions, (b)heavy ions (c) relative drifts between heavy and light ions due to their ExB drifts, (d) same as (c) but due to their polarization drifts, and ((e) drifts of electrons from R-4. The time period shown in these panels cover the large-amplitude burst of electrostatic noise in Figure 6a.

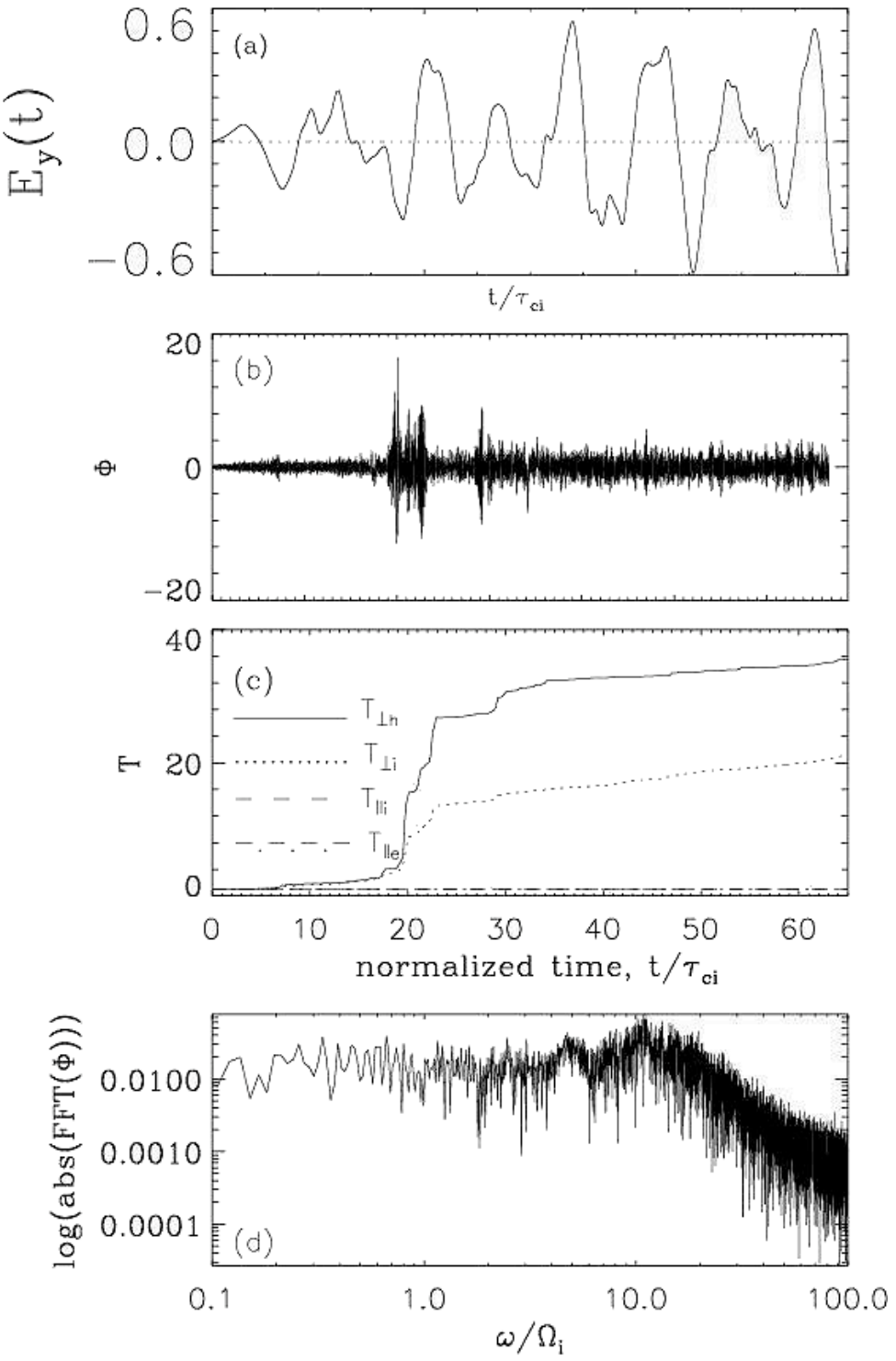

Figure 8. Same as Figure 6, but from R-5 in which the exponent in the power law spectrum is □=-2.